Supporting Information

for

Magnetic Sensing Potential of Fe_3O_4 Nanocubes Exceeds That of Fe_3O_4 Nanospheres

Arati G. Kolhatkar,[†] Yi-Ting Chen,[†] Pawilai Chinwangso,[†,‡] Ivan Nekrashevich,[‡] Gamage C. Dannangoda,[§] Ankit Singh,[∥] Andrew C. Jamison,[†] Oussama Zenasni,[†] Irene A. Rusakova,[⊥] Karen S. Martirosyan,[*,§] Dmitri Litvinov,[*,†,‡,∥] Shoujun Xu,[*,†] Richard C. Willson,[*,∥] and T. Randall Lee[*,†]

[†]*Department of Chemistry and Texas Center for Superconductivity,* [‡]*Department of Electrical and Computer Engineering,* [∥]*Department of Chemical and Biomolecular Engineering, and* [⊥]*Department of Physics and Texas Center for Superconductivity, University of Houston, 4800 Calhoun Road, Houston, Texas 77204, United States*

[§]*Department of Physics, University of Texas Rio Grande Valley, Brownsville, Texas 78520, United States*

Corresponding Authors

*Email: karen.martirosyan@utrgv.edu (K.S.M.); litvinov@uh.edu (D.L.); sxu7@central.uh.edu (S.X.); willson@uh.edu (R.C.W); trlee@uh.edu (T.R.L.).

Table S1. Comparison of Magnetic Properties of Various Shapes of Nanoparticles. Reproduced from Kolhatkar *et al.*[1]

Reference	MNP	Shape	Size (nm) Volume comparison	Saturation Magnetization (Ms, emu/g)	Coercivity	Blocking Temperature (T_B, K)
Montferrand, C. *et al.*[2]	Fe_3O_4 (includes γFe_2O_3)	Cube Rod Sphere Octahedron	12 Side 12 Width 12 12 Width $V_{cube} > V_{rod} > V_{sphere} > V_{octahedron}$	40 18 80 80	0 4.4 kA/m 0 0	
Song, Q. *et al.*[3]	$CoFe_2O_4$	Sphere Cube	10 8 $V_{sphere} = V_{cube}$	80 80	16000 Oe 9500 Oe	275 275
Salazar-Alvarez, G. *et al.*[4]	γFe_2O_3	Sphere Cube	14.5 12 Side $V_{sphere} = V_{cube}$	75 75	30 mT 33 mT	235 190
Chou, S. *et al.*[5]	FePt	Cube Octapod Cuboctahedron	11.8 12 body dia 6.8 dia $V_{cube} > V_{octapod} > V_{octahedron}$	2.5 2.0 0.1	164 Oe 1461 Oe 11 Oe	50 95 20
Zhen, G. *et al.*[6]	Fe_3O_4	Cube Sphere	8.0 Side 8.5 $V_{cube} > V_{sphere}$	40 31	0 0	60 100
Noh, S. *et al.*[7]	$Zn_{0.4}Fe_{2.6}O_4$	Sphere Cube	22 18 $V_{sphere} = V_{cube}$	145 165	0 0	360 320

We calculated the crystallinity index (CI) for each of our nanocubes and nanospheres using the following equation.

$$CI = [(\text{MNP size by SEM/TEM})/(\text{Crystallite size})] \quad (1)$$

Note: a crystallinity index close to 1 indicates a crystal that is completely monocrystalline.

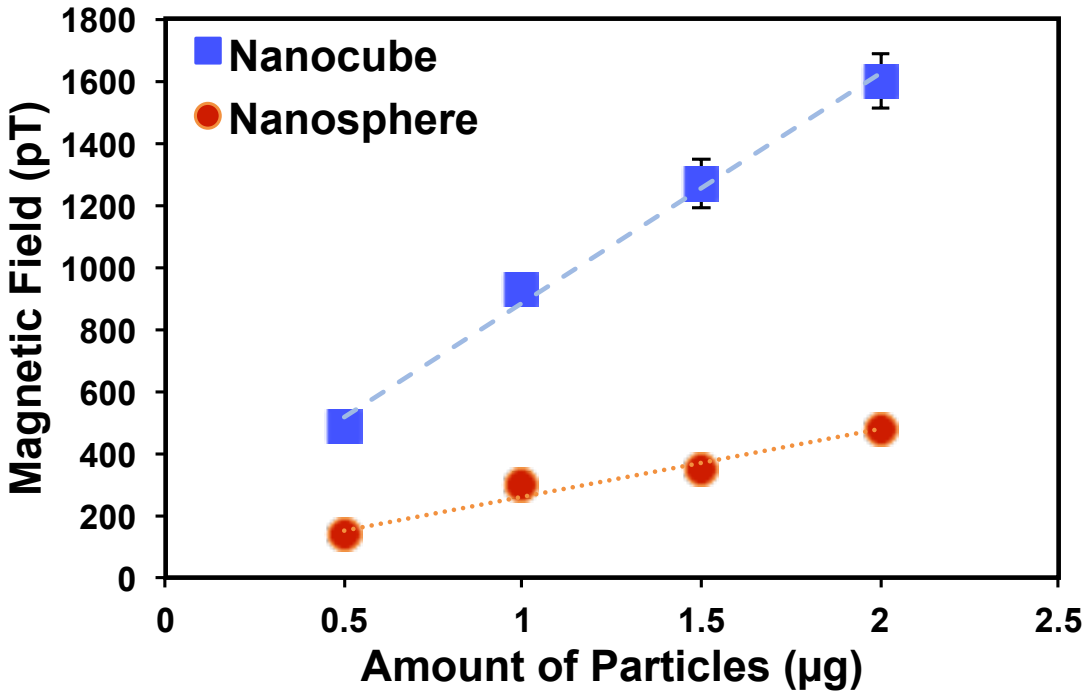

Figure S1. Quantification of magnetic signal as a function of magnetic nanoparticle mass.

Table S2. Crystallite Size and the Crystallinity Index for Fe_3O_4 Nanocubes and Nanospheres

MNP Shape	Size (nm)	Crystallite Size (nm)	Crystallinity Index
Cube	135	43	3
	150	56	4
	175	43	4
	225	57	5
Sphere	100	17	6
	125	13	10
	135	17	8
	150	15	13
	175	12	15
	275	11	26

Average crystallite size of cubic MNPs is 50 ± 8 nm and the crystallinity index is 4 ± 1. In contrast, average crystallite size of spherical MNPs is 14 ± 3 nm and crystallinity index is 17 ± 7 nm.

Giant Magnetoresistance (GMR) Sensor Fabrication

Giant magnetoresistance (GMR) multilayers of Ta(5nm)/Co(5nm)/Cu(3nm)/Co(5nm)/Ta(nm) were deposited in an AJA-2200 ultra-high vacuum magnetron sputtering system at a base pressure of 2×10^{-8} Torr. Silicon wafers coated with 500 nm of thermal oxide were used as substrates. The deposition was conducted at 2.5 mTorr Ar pressure at room temperature. The deposition rates of copper, cobalt, and tantalum were 2.6 Å/s, 0.59 Å/s, and 1 Å/s, respectively. The multilayer films were patterned into 3 × 4 sensor arrays with Cu leads added to probe the individual sensors. A combination of conventional e-beam and optical lithography techniques was used for device patterning, and the resulting sensor array was coated with a 25 nm of amorphous alumina for corrosion protection in nanoparticle-sensing experiments.[8] An SEM image of a sensor array with 300 nm × 1.5 μm sensors is shown in Figure S2.

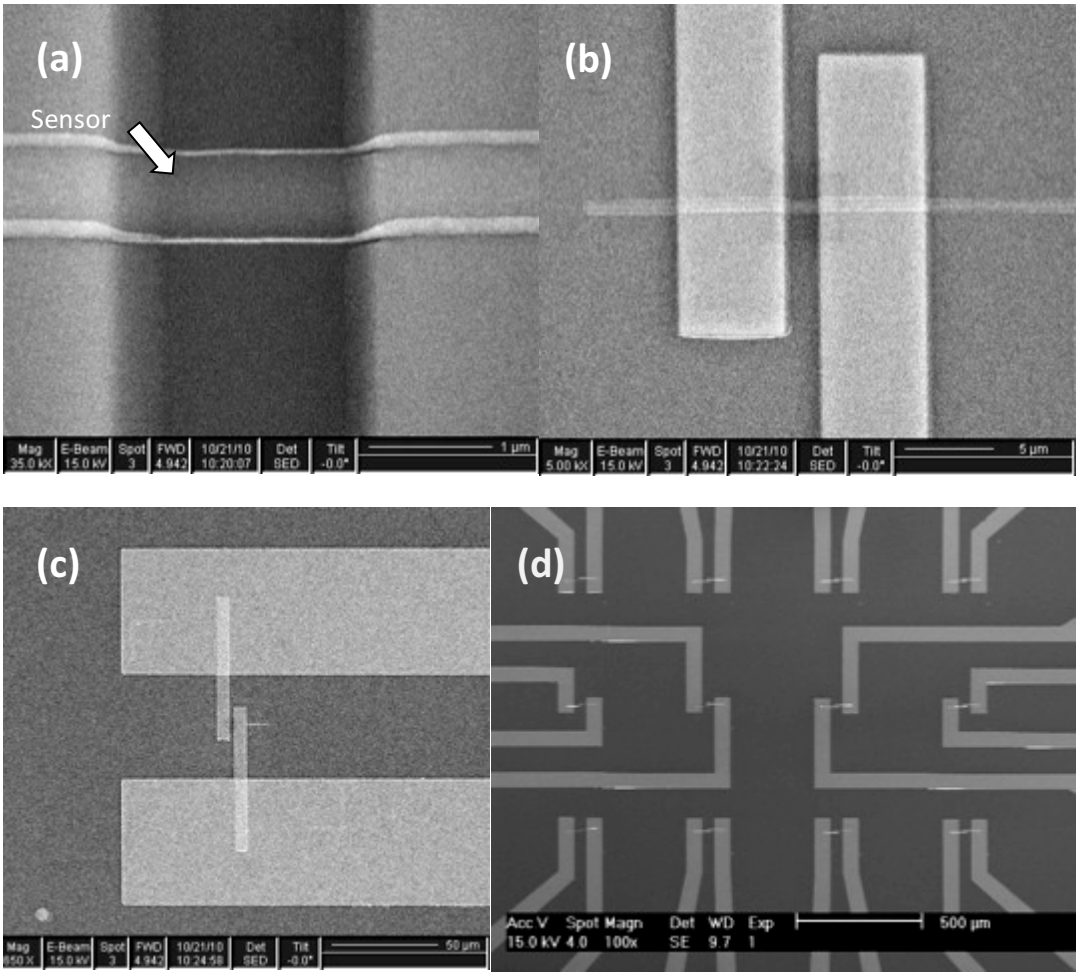

Figure S2. SEM images of the sensor array at different levels magnifications from (a) being the highest magnification/zoom showing individual sensor to (d) being the lowest magnification/zoom showing the entire sensor array.

References

(1) Kolhatkar, A.G.; Jamison, A.C.; Litvinov, D.; Willson, R.C.; Lee, T.R. Tuning the Magnetic Properties of Nanoparticles. *Int. J. Mol. Sci.* **2013**, *14*, 1–34.

(2) de Montferrand, C.; Hu, L.; Milosevic, I.; Russier, V.; Bonnin, D.; Motte, L.; Brioude, A.; Lalatonne, Y. Iron Oxide Nanoparticles with Sizes, Shapes and Compositions Resulting in Different Magnetization Signatures as Potential Labels for Multiparametric Detection. *Acta Biomater.* **2013**, *9*, 6150-6157.

(3) Song, Q.; Zhang, Z.J. Shape Control and Associated Magnetic Properties of Spinel Cobalt Ferrite Nanocrystals. *J. Am. Chem. Soc.* **2004**, *126*, 6164-6168.

(4) Salazar-Alvarez, G.; Qin, J.; Sepelak, V.; Bergmann, I.; Vasilakaki, M.; Trohidou, K.N.; Ardisson, J.D.; Macedo, W.A.A.; Mikhaylova, M.; Muhammed, M.; Baro, M.D.; Nogues, J. Cubic versus Spherical Magnetic Nanoparticles: The Role of Surface Anisotropy. *J. Am. Chem. Soc.* **2008**, *130*, 13234-13239.

(5) Chou, S.-W.; Zhu, C.-L.; Neeleshwar, S.; Chen, C.-L.; Chen, Y.-Y.; Chen, C.-C. Controlled Growth and Magnetic Property of FePt Nanostructure: Cuboctahedron, Octapod, Truncated Cube, and Cube. *Chem. Mater.* **2009**, *21*, 4955-4961.

(6) Zhen, G.; Muir, B.W.; Moffat, B.A.; Harbour, P.; Murray, K.S.; Moubaraki, B.; Suzuki, K.; Madsen, I.; Agron-Olshina, N.; Waddington, L.; Mulvaney, P.; Hartley, P.G. Comparative Study of the Magnetic Behavior of Spherical and Cubic Superparamagnetic Iron Oxide Nanoparticles. *J. Phys. Chem. C* **2011**, *115*, 327-334.

(7) Noh, S.-h.; Na, W.; Jang, J.-t.; Lee, J.-H.; Lee, E.J.; Moon, S.H.; Lim, Y.; Shin, J.-S.; Cheon, J. Nanoscale Magnetism Control via Surface and Exchange Anisotropy for Optimized Ferrimagnetic Hysteresis. *Nano Lett.* **2012***, 12*, 3716-3721.

(8) Litvinov, J.; Wang, Y.-J.; George, J.; Chinwangso, P.; Brankovic, S.; Willson, R.C.; Litvinov, D. Development of Pinhole-Free Amorphous Aluminum Oxide Protective Layers for Biomedical Device Applications. *Surf. Coat. Technol.* **2013**, *224*, 101-108.